Journal of the European Ceramic Society 19 (1999) 2475–2485

PII: S0955-2219(99)00095-3
0955-2219/99/$ - see front matter

Creep Behaviour of Al_2O_3–SiC Nanocomposites

P. Descamps, [a]* D. O'Sullivan, [b†] M. Poorteman, [a] J. C. Descamps, [c] A. Leriche [b] and F. Cambier [a]

[a]Belgian Ceramic Research Centre, Avenue Gouverneur Cornez, 4, 7000 Mons, Belgium
[b]LAMAC, Université de Valenciennes, ZI Champ de l'Abbesse, 59600 Maubeuge, France
[c]Department of Materials Science, Faculté Polytechnique de Mons, 7000 Mons, Belgium

Abstract

Compared with monolithic fine grained Al_2O_3, Al_2O_3 nanocomposites reinforced with SiC nanoparticles display especially high modulus of rupture as well as reduced creep strain. Taking into account the fracture mode change, the morphology of ground surfaces showing plastic grooving, the low sensitivity to wear and the low dependence of erosion rate with grain size, it can be reasonably assumed that the strength improvement is associated with an increase of the interface cohesion (due to bridging by SiC particles) rather than with a grain size refinement involving substructure formation (as initially suggested by Niihara). In the present work, creep tests have been performed and the results agree with such a reinforcement of the mechanical properties by SiC particle bridging Al_2O_3–Al_2O_3 grain boundaries. Indeed, particles pinning the grain boundaries hinder grain boundary sliding resulting in a large improvement in creep resistance. In addition, SiC particles, while counteracting sliding, give rise to a recoverable viscoelastic contribution to creep. Because of the increased interface strength, the samples undergoing creep support stress levels, greater than the threshold value required to activate dislocation motion. The high stress exponent value as well as the presence of a high dislocation density in the strained materials suggests that a lattice mechanism controls the deformation process. Finally, a model is proposed which fits well with the experimental creep results. © *1999 Elsevier Science Ltd. All rights reserved.*

Keywords: creep, nanocomposites, Al_2O_3, SiC, mechanical properties.

1 Introduction

Since the work of Niihara and his co-workers[1,2] there is a strong interest in the concept of nanocomposites which involves the incorporation of nano-size particles (typically 100 nm or less) into a host matrix.

These authors reported that the dispersion of 5 vol% silicon carbide into an Al_2O_3 matrix results in a large enhancement of the fracture strength and, for a lesser extent, of the toughness. The high strength value is maintained up to 1200°C[3] and furthermore, the Al_2O_3–SiC nanocomposite is characterised by a markedly improved creep resistance (several order of magnitude) compared with monolithic alumina.[4]

Some attempts to explain such an improvement of the thermo-mechanical properties and of the creep resistance have been proposed in literature.

Initially, Niihara associated the fracture strength increase with a decrease of the critical flaw size, due to dislocation sub-grain structure formation, giving rise to a microstructural refinement.[2] However, this model is unrealistic as the size of the flaw calculated according with Irwin–Griffith relationship (assuming a flaw of semi-circular shape located close to the surface) remains larger than the sub-grain size but also larger than the size of alumina grain free of dislocations.

Assuming a very sharp rising *R*-curve effect,[5] as well as a strong Al_2O_3/SiC interfacial bond, Ohji *et al.*[6] have proposed a reinforcement mechanism based on a crack shielding effect which occurs when intra-granular particles bridge a propagating crack, just behind the crack tip. Following this model, the crack–SiC grain interaction requires thermally induced tensile stresses at the interface to allow the crack to propagate toward the particle. However, this model does not apply at high temperature, as it cannot explain why the improvement of the mechanical properties resulting from the nano particles addition is maintained whereas thermal stresses are relaxed. Moreover, Transmission Electron Microscopy (TEM) observations performed on indented specimens proved that there is very rare interaction between the main crack and intra-granular SiC particles.

As an alternative explanation, Levin *et al.*[7] have proposed a mechanism which is the result of both a

*To whom correspondence should be addressed.
†Present address: Materials Science Department, University of Limerick, Limerick, Ireland.

matrix weakening and a grain boundary strengthening. Following these authors, the thermal expansion mismatch between Al_2O_3 and SiC leads to the development of residual tensile micro-stresses into alumina grains and radial compressive micro-stresses at grain boundaries (clamping stresses). As a consequence, crack preferentially deflects through the grain which is confirmed by fracture face analysis. Unfortunately, this mechanism, even if supported by the works of some authors,[8] is again unable to account for the higher modulus of rupture measured at elevated temperature.

Another hypothesis, also based on grain boundary strengthening, but which better fits with the reported thermo-mechanical properties as it is less temperature dependent, is based on the formation of very strong Al_2O_3–intergranular SiC bonds. Such strong interfacial bonds can be attributed, first, to the lack of residual glassy phase (which is squeezed out during the cooling step of the firing process) and, secondly, to lattice matches in many Al_2O_3/SiC interfaces.[9]

The increase of the grain boundary strength is confirmed by the following experimental features:

- a change from an intergranular to a transgranular fracture mode proving that the crack propagates through Al_2O_3 grains;[5]
- when grinding, cutting effects with grooves formation becomes predominant over micro-cracking and pull out (as it is the case for the alumina matrix) and the surface can undergo higher compressive stress[10] (as a consequence, samples ground using a 800 mesh diamond wheel display higher strength values than polished ones: an increase of 34% has been recorded on materials discussed in this paper);
- the nanocomposite displays a better resistance to erosion and, in addition, the wear rate appears to be less grain size dependent.[11]

Taking the above features into account, it is believed that intergranular SiC particles very likely play a major role in the improvement of the mechanical properties of nano composites. Therefore, the scope of the present paper is to assess the effect of those bridging SiC grains on the creep behaviour.

2 Experimental Procedure

2.1 Processing

Al_2O_3 (AKP 53, Sumitomo, Japan) matrix, containing 5 vol% of SiC (UF45, HC Starck, Germany) nano phase (0·26 μm) was processed as follows:

- Aqueous slurries of both the matrix and the secondary phase powders were first separately dispersed by mechanical stirring (Al_2O_3) or by ultrasonic agitation (SiC).
- The pH of the slurries was adjusted to >11 in order to obtain suspensions where both the Al_2O_3 and the SiC reached their lowest negative zeta potential values, therefore allowing mutual repulsion between particles in the separate as well as in the mixed suspensions.
- The two slurries were mixed, ultrasonically agitated and vibration milled for 16 h using Al_2O_3 cylinders as the grinding media.
- The mixed slurry was dried by freeze drying. Finally the Al_2O_3/SiC mixed powder was hot pressed at 1550°C, under 40 MPa, for 30 min, in Ar. As a consequence of the processing route, the impurity content detected by ICP significantly increased (Si: 65→861 ppm; Mg: 12→46 ppm), due to erosion of the grinding media and to the thin silica layer covering SiC nanoparticles.

In order to assess any creep improvement resulting from SiC nanophase addition, a reference sample was fabricated from unprocessed Al_2O_3 powder.

Taking into account that particles of the secondary phase hinder grain growth, the hot pressing temperature was reduced to 1400°C to obtain a monolithic Al_2O_3 material having almost the same Al_2O_3 grain size as that of the nano composite.

It must be emphasised that the Al_2O_3 raw material was hot pressed as-received with the goal of obtaining a highly pure sintered material (almost free of residual glassy phase), which would have a creep resistance as high as possible for that system (in spite of its small grain size).

2.2 Characterisation of the sintered samples

Hot pressed monolithic Al_2O_3 and Al_2O_3–SiC nanocomposite samples have been characterised in terms of microstructure and of creep behaviour.

The microstructures of both materials have been revealed by TEM observation of carbon-coated foils previously thinned by ion milling. In order to detect microstructural changes associated with the creep deformation process in both the monolithic Al_2O_3 and the nanocomposite, specimens were prepared from as-fired materials and from materials which had undergone creep.

The creep behaviour of both the Al_2O_3 monolith and the nanocomposite was assessed in three-point bending (Zwick 1474 universal testing machine) on bars (dimension: $3\times4\times35$ mm^3) using an Al_2O_3 flexural jig having a 30 mm span.

The displacement of the centre of the sample was measured throughout the test using a linear variable displacement transducer with a precision of less than 1 μm. Creep tests were carried out on a universal testing machine fitted with a close loop regulation unit coupled to a function generator which allows very close control of the applied load to be maintained.

The bending stresses σ_{max} and the strain rate $\dot{\varepsilon}_{max}$ were calculated according to relationships derived from Hollenberg's analysis:[12]

$$\sigma_{max} = \frac{3PS}{2bh^2}\left(\frac{2n+1}{3n}\right) \quad (1)$$

$$\dot{\varepsilon}_{max} = \frac{2h}{S^2}(n+2)\dot{Y}_{max} \quad (2)$$

where P is the applied stress, S is the span between the support rollers, h is the specimen thickness, b is the specimen width, n is the stress exponent and $\dot{Y}_{max}$ is the rate of displacement at the centre part of the specimen.

The creep parameters (stress exponent n and activation energy Q) were measured using stress and temperature jumps techniques. These techniques require a sudden change of either the applied stress or the temperature during a single test and the measurement of the strain rate just before and immediately after the jump.

3 Results and Discussion

3.1 Microstructural observation of as-sintered materials

TEM micrographs of the monolithic Al_2O_3 clearly showed that the grain size distribution was bimodal, with some coarser grains (typically 2 μm) present into a sub-micron size matrix (Fig. 1).

In these coarser grains, dislocations were occasionally observed. Even at higher magnification, no glass pockets were detected. This can be viewed as the consequence of the very pure Al_2O_3 raw material used.

Despite this higher sintering temperature, the nanocomposite microstructure was also very fine but the grain size distribution appeared more uniform than the monolithic Al_2O_3 (Fig. 2). This fine microstructure, resulted from intergranular SiC nanoparticles pinning the grain boundaries (Zener pinning) and reducing their mobility (as confirmed by grain boundary bowing at SiC grains). As a consequence, grain growth was necessarily lowered. When located in intragranular positions, SiC nanoparticles were sometime associated with dislocations (Fig. 3) whose density seemed higher than for the monolithic Al_2O_3.

A very small number of glassy pockets were observed at triple points in the nanocomposite microstructure.

3.2 Creep assessment

3.2.1 Comparison between the creep resistance of the monolithic and the nanocomposite

The creep resistances, of both the monolithic Al_2O_3 and of the nanocomposite were determined under a 100 MPa load at temperatures ranging from 1200 to 1350°C (Fig. 4). At 1300°C, the monolith deformation occured so rapidly that the transducer limit (≈1 mm) was exceeded after 30 min and only

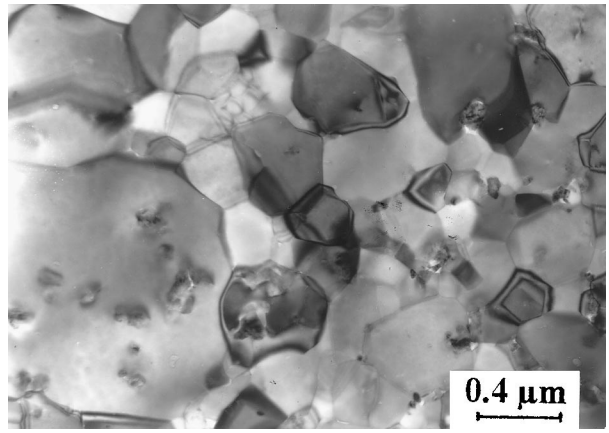

Fig. 2. TEM micrograph of the nanocomposite microstructure prior to creep showing both inter and intragranular SiC.

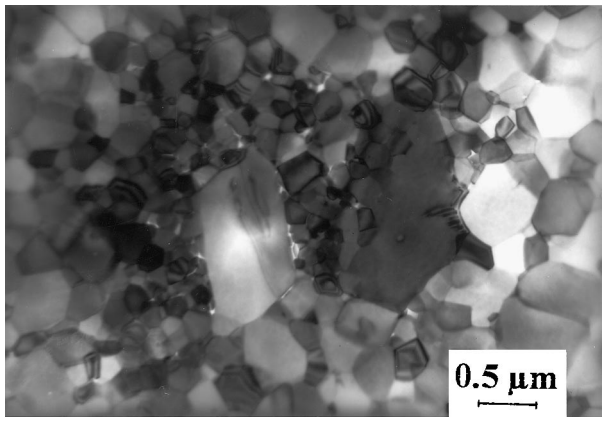

Fig. 1. TEM micrograph of monolithic alumina microstructure prior to creep.

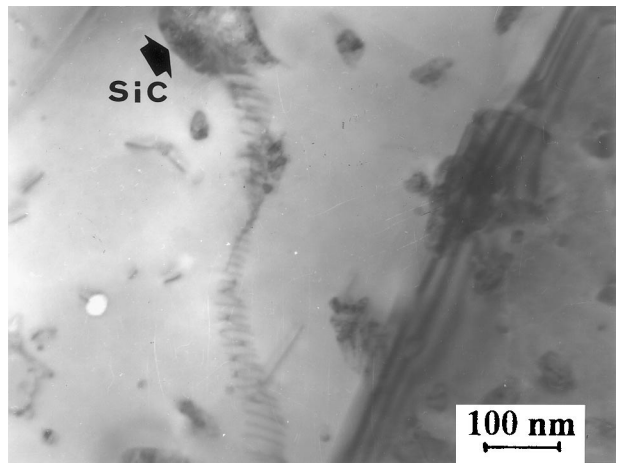

Fig. 3. TEM micrograph of nanocomposite showing dislocations associated with intragranular SiC particles.

primary creep was recorded. On the other hand, at the same temperature, deformation of the nanocomposite was considerably lower and no clear steady state seemed to be reached. However, at a same stress but at a slightly higher temperature (1350°C) the steady-state creep was attained. Figure 4 clearly demonstrated that it was necessary to increase the testing temperature of the nanocomposite by at least 150°C in order to obtain similar creep behaviour to that of the monolith.

3.2.2 Stress relaxation tests performed at elevated temperature

In contrast to the monolith for which only instantaneous elastic recovery (sum of the elastic deformation of the specimen and of the testing machine) took place once the stress was removed, the nanocomposite also displayed a slow asymptotic recovery characteristic of a viscoelastic effect and which very likely accounts for the extended primary creep and for the delay of the steady state creep stage (Fig. 5). Such an anelastic recovery has already been observed for SiC whisker-reinforced Al_2O_3 material.[13,14] In that case, the recovery was attributed to an interconnecting network of whiskers which develops during processing[14] over a percolation threshold which corresponds to 15 vol% of SiC whiskers.

3.2.3 Study of the viscoelastic phenomenon

A threshold stress was identified in the creep test on the nanocomposite (between 20 and 25 MPa for tests carried out at 1300°C), below which no permanent deformation occurred. The displacement versus time curve at stresses below the threshold

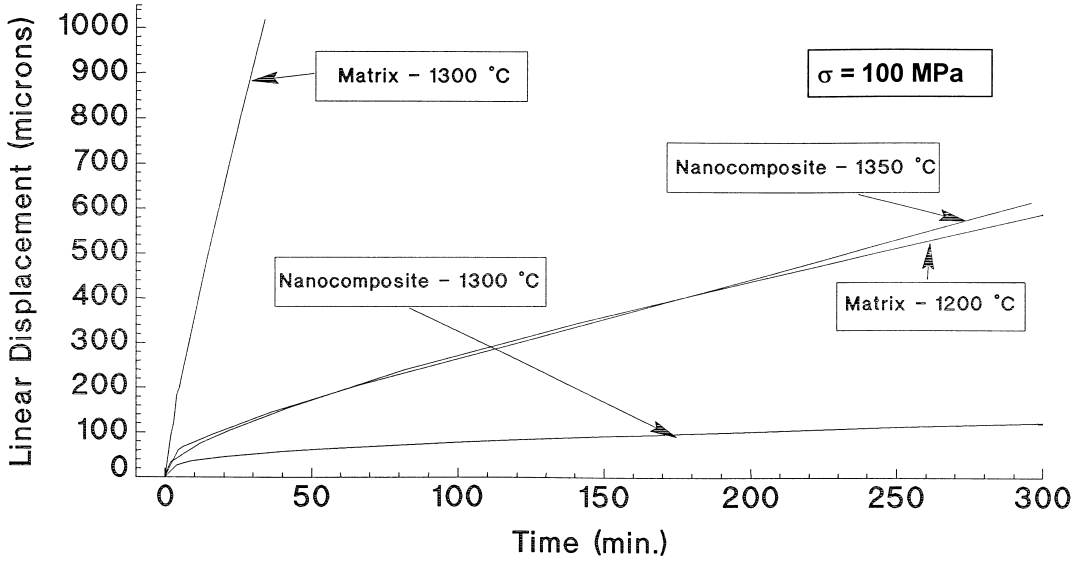

Fig. 4. Flexural creep behaviour of monolithic alumina and nanocomposite under a stress of 100 MPa and a temperature ranging from 1200 to 1350°C.

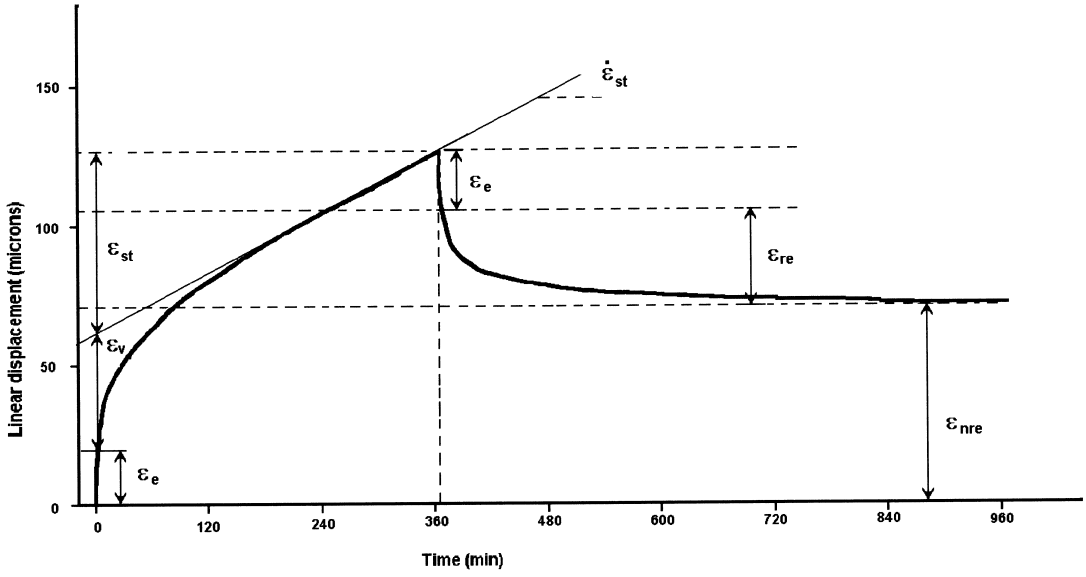

Fig. 5. Typical recorded creep and recovery curve and the nomenclature used to describe the various strains involved.

stress was very similar to that of Kelvin–Voigt (K–V) viscoelastic model.[15]

In fact, it is believed that this simple model for creep and recovery which basically consists of a spring and a dashpot in parallel can reasonably explains the creep events at a grain boundary bridged by a SiC particle.

Taking into account the presence of a residual glassy phase at the grain boundaries, the K–V element can be related to grain boundary sliding impeded by a pinning SiC particle. Indeed, during the creep test, the shear stress component allowed grain boundary sliding to occur at a velocity which depended on the glass viscosity, i.e. the dashpot viscosity in the K–V model. If the grain boundary is considered to be pinned by an SiC particle, the sliding process can only take place if the particle deforms elastically. This elastic deformation corresponds to the spring in the K–V model and is in parallel with the dashpot to take into account that intergranular SiC particles tend to counteract grain boundary sliding.

According to this viscoelastic model, the strain variation as a function of time is given by the following relationships:

$$\varepsilon_V(t) = \frac{\tau}{G}\left(1 - \exp(-\frac{t}{\lambda})\right) \tag{3}$$

during loading, and

$$\varepsilon_{VU}(t) = \frac{\tau}{G}\exp\left(\frac{-t - t_u}{\lambda}\right) \tag{4}$$

once the load removed;

where G is the spring constant, τ the shear component of the stress, t_u the time under load and λ the necessary time for recovery to be completed (retardation time) defined as $\lambda = \eta/G$ where η is the dashpot viscosity.

Thus, a plot of $\ln(\varepsilon_{Vu}(t))$ against t should yield a straight line, which is in contradiction with the experimental results. Therefore, the nanocomposite behaviour could not be represented by such a simple model.

In fact, the discrepancy very likely arose because the K–V element, only models a single grain boundary pinned by a SiC particle.[16] Since the bulk of the material contains many of these K–V elements, each having its own characteristic relaxation time, the summation of these elements requires the introduction of a spectrum of retardation times[17] and eqn. (3) becomes:

$$\varepsilon_V(t) = \Sigma_i \varepsilon_{Vi}(t) = \tau\Sigma\frac{1}{G_i}\left(1 - \exp(-\frac{t}{\lambda_i})\right) \tag{5}$$

On this basis, the Inokuchi analysis[18] has been adopted. Using this iterative procedure, it is possible to assess values of G_i and λ_i in the general viscoelastic relationship and to define the number of K–V elements necessary to obtain a good fit between the mathematically rebuilt curve and the experimentally measured recovery curve.

As confirmed by Fig. 6, two K–V elements in series enables the accurate modelling of the viscoelastic contribution to the creep strain. However, if

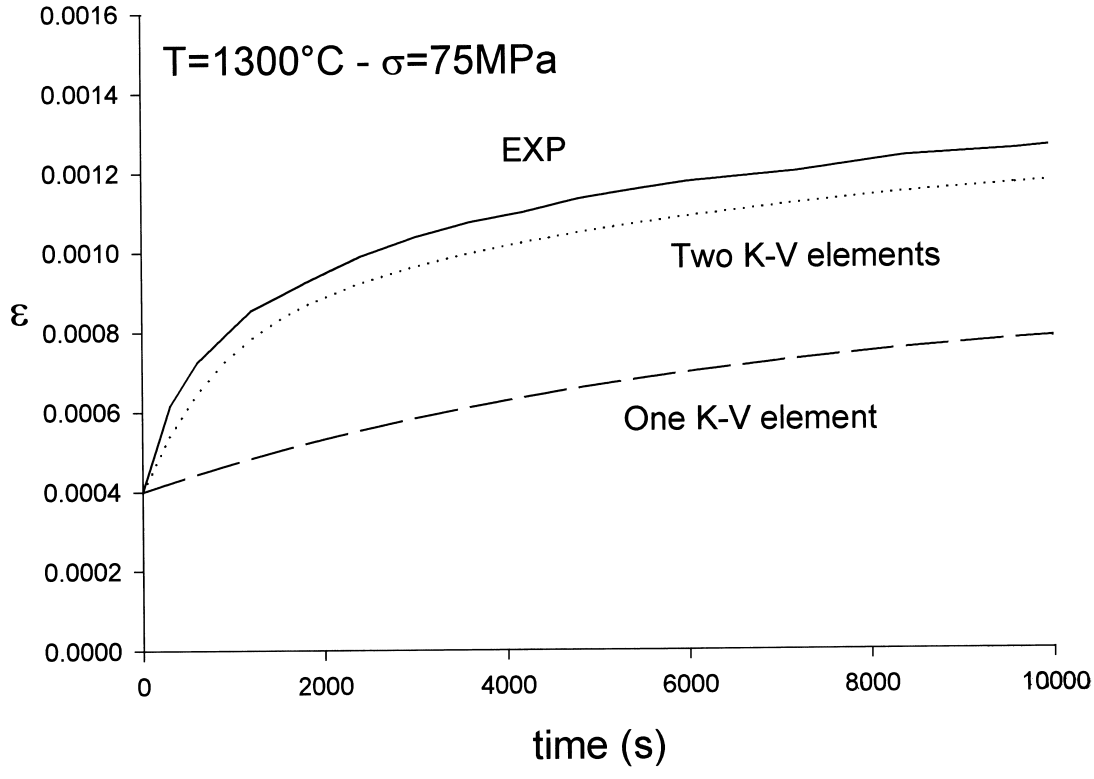

Fig. 6. Experimental recovery curve and curve rebuilt from Inokuchi mathematical analysis.

viscoelasticity (ε_v) is the only additional contribution to elastic (ε_e) and permanent steady-state (ε_{st}) strains, the recovery curve must be the same as the primary curve after subtraction of ε_e and ε_{st} (Fig. 5). Thus

$$\varepsilon(t) - \varepsilon_e - \dot{\varepsilon}_{st}.t \tag{6}$$

on loading is necessarily equal to

$$\varepsilon_{re} + \varepsilon_{nre} - \varepsilon(t - t_u) \tag{7}$$

during recovery (where ε_{re} is the fully recovered deformation and ε_{nre} is the unrecovered plastic strain expressed as $\dot{\varepsilon}_{st} \cdot t_u$).

However, successive loading–unloading cycles during a single experiment showed that the above equality was satisfied starting from the third cycle (Fig. 7). It can also be observed that, when increasing the number of cycles, the sample stiffness increases as the elastic strain component, ε_e, slightly decreases. Both of these findings undoubtedly highlight the fact that, in addition, to ε_e, ε_{st} and ε_V another transient unrecoverable phenomenon takes part in the deformation process. This fourth creep contribution will be discussed hereafter on the basis of microstructural analysis of samples which had undergone creep testing.

3.2.4 *Study of the secondary creep mechanism*

The stress exponent (n) and the apparent activation energy (Q) of the monolithic Al_2O_3 and the nanocomposite were measured from log $\dot{\varepsilon}$ versus log σ and ln $\dot{\varepsilon}$ versus $1/T$ plots shown in Figs 8 and 9. As previously stated, the data for these plots were obtained using stress and temperature jump experiments. Compared with the monolith, much higher testing temperatures have been adopted for

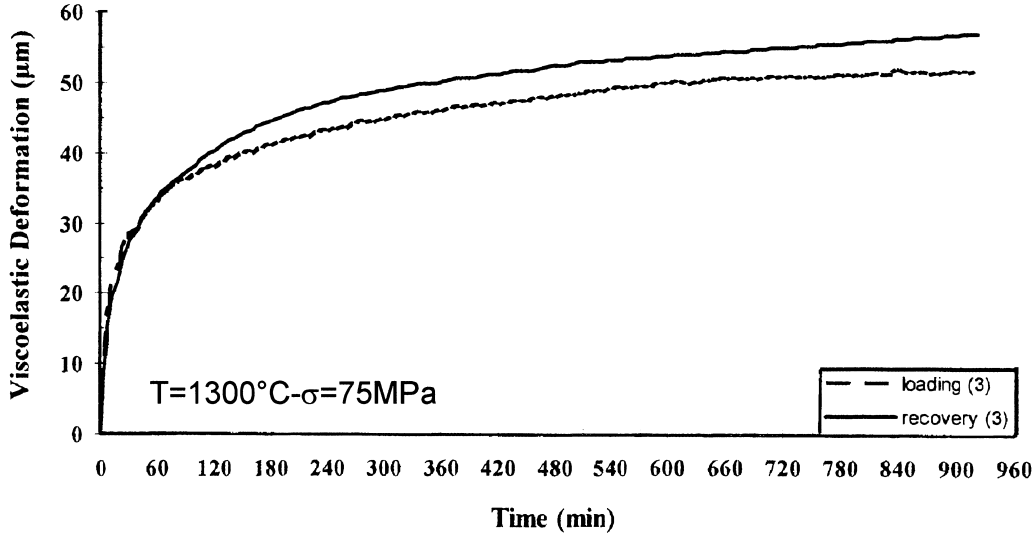

Fig. 7. Fitting between the third cycle recovery curve and the third cycle primary curve after subtraction of elastic and permanent strains.

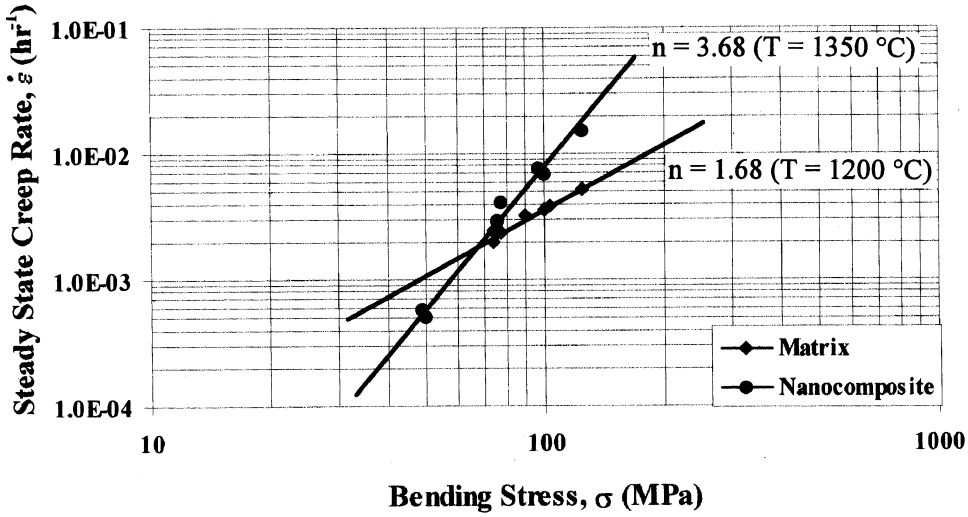

Fig. 8. Strain rate ($\dot{\varepsilon}$) of monolithic alumina (1200°C) and of nanocomposite (1350°C) versus applied stress.

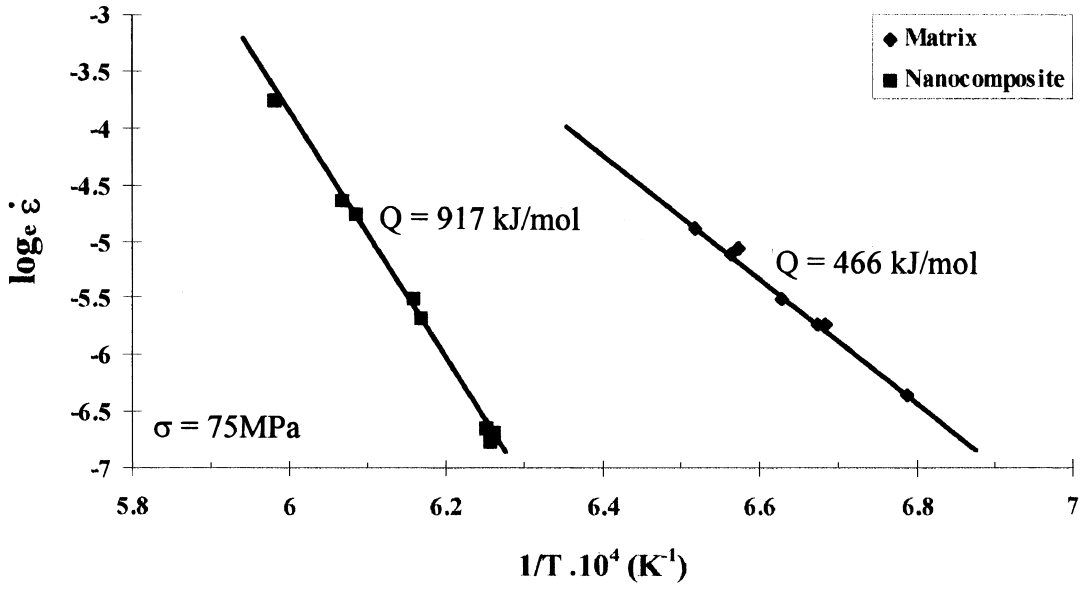

Fig. 9. Strain rate (ε) versus inverse temperature for the matrix and the nanocomposite ($\sigma = 75$ MPa).

the nanocomposite. The reason is that, at those temperatures, the kinetic of the primary creep mechanism becomes fast enough for stationary creep to be reached. Under the selected creep conditions, straight lines were obtained and, in addition, the scatter in the results was low indicating that the viscoelastic contribution did not affect the steady-state strain rates.

Therefore, it can be assumed that the jump techniques yielded reliable values of the creep parameters.

The monolithic Al_2O_3 stress exponent ($n = 1{\cdot}68$) was fully in agreement with previously reported values.[19–22] However, the nanocomposite displayed an especially high value ($n = 3{\cdot}68$) that could not be explained simply by the presence of a threshold stress below which the mechanism responsible for permanent strain did not take place. In addition, the activation energy of the nanocomposite ($Q = 917$ kJ mol^{-1}) was almost twice that of the monolithic material ($Q = 466$ kJ mol^{-1}). Such creep parameter values, although quite high for an alumina based ceramic composite have already been obtained in the case of whisker-or platelet-reinforced oxide matrices.[21–23]

3.3 TEM examination of specimens after creep

No difference in the dislocation densities of monolithic Al_2O_3, before and after creep, was observed by TEM.

The main feature observed was the large number of pores, particularly at triple junctions in the material after creep (Fig. 10). As creep proceeded these pores grew into finger-like cavities and, if creep would be allowed to continue, their interlinking would give rise to premature failure of the sample.

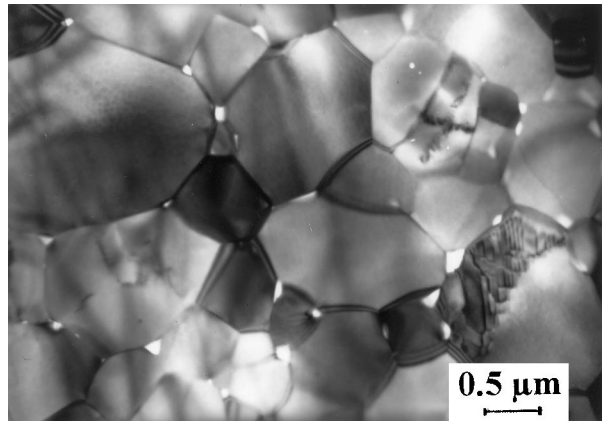

Fig. 10. TEM micrograph of monolithic alumina after creep showing extensive cavitation mainly at triple junctions.

Early nucleation and subsequent growth of cavities suggests that, during deformation, grain boundary sliding occured very rapidly. Therefore, stress concentrations, mostly at triple points, could not be relaxed by conventional accommodation mechanisms resulting in a low creep strength and a rapidly attained tertiary creep stage.

On the other hand, the nanocomposite microstructure contained very few cavities (Fig. 11). In fact, cavity nucleation seems to be associated with intergranular SiC nanoparticles and with matrix grain boundaries free of SiC particles.

In the first case, voids were formed due to forced rotation of SiC particles which impede grain boundary sliding.[4] This observation confirms the viscoelastic contribution to creep. In the second case, due to the absence of SiC particles at particular grain boundaries and to the presence of a thin glassy phase layer, indicated by an arrow in Fig. 12, the shear stress component allowed sliding to easily occur whereas the tensile component favoured grain

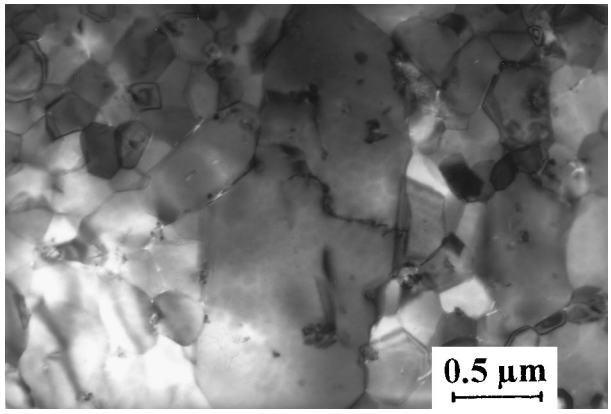

Fig. 11. TEM micrograph of the nanocomposite after creep.

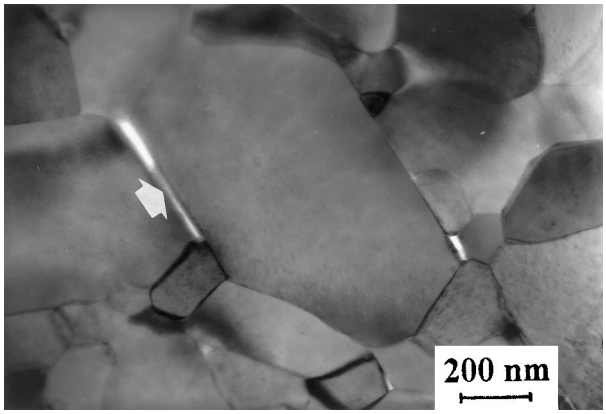

Fig. 12. TEM micrograph of nanocomposite showing crack-like cavities at grain boundaries free of SiC bridging particles.

boundary opening. The combination of the two stress components promoted cavitation. Taking into account that cavity nucleation preferentially arose along grain boundaries free of SiC particles, it can reasonably be assumed that such grain boundaries have a lower cohesion than SiC bridged Al_2O_3 grain boundaries. As noted by several authors,[9,24] this implies that silicon carbide-alumina interfaces are more strongly bonded than alumina–alumina interfaces.

Enhancement of grain boundary cohesion prevents grain boundary sliding and secondly introduces a viscoelastic effect which agrees with the experimental results.

Figure 13 shows that where substantial sliding occurred, some grains were forced into their neighbours causing deformation in the latter and also giving rise to dislocation motion in the deformed grains.

This undoubtedly demonstrates that the nanocomposite supported stresses higher than the threshold value above which dislocation motion started to occur and plastic deformation of the grain by a lattice mechanism allowed stresses associated with the sliding of neighbours to be accommodated.

The high n value measured (see Section 3·2) is a common feature of mechanisms involving dislocation motion ($n = 3$ or 5 depending on whether the deformation process is controlled by dislocation glide or climb, respectively[25,26]). Such a value also supports the assumption that dislocation motion played a major role in the permanent creep stage. Finally, as mentioned by Niihara, grain substructure formation due to linking up of dislocation has been identified. However, such substructure formation responsible for grain refinement was very rare and therefore is not a significant part of either the improvement in room temperature mechanical properties or of the creep process.

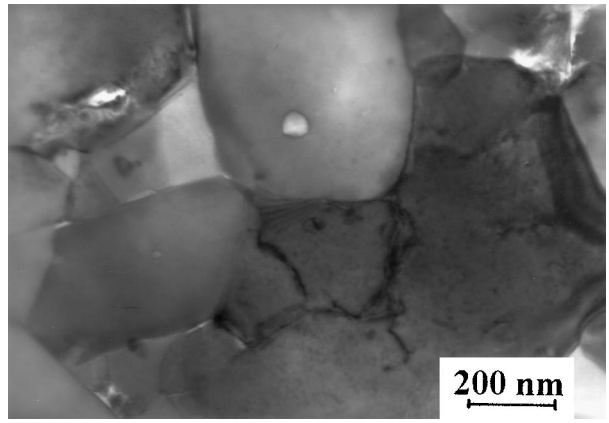

Fig. 13. TEM micrograph of nanocomposite after creep showing the presence of deformed grains due to plastic accommodation of grain boundary sliding.

3.4 Proposal of a deformation mechanism for the nanocomposite

According to Lange *et al.*,[27] any deformation process can be represented by a sum of three concurrent mechanisms each contributing to the total creep ε_t and, the strain relationship can be expressed by: $\varepsilon_t = \varepsilon_V + \varepsilon_p + \varepsilon_{\text{cav}}$ where ε_V is the viscoelastic deformation, ε_p the permanent strain (i.e. diffusion mechanisms, lattice mechanisms...) and ε_{cav} the deformation associated with cavity formation. For nanocomposites, creep experiments involving three successive loading–unloading cycles showed recovery to be essentially independent of the accumulated strain, which indicates that viscoelastic and permanent creep mechanisms can be effectively treated separately.

During creep tests, the samples underwent low strains and as a consequence the level of cavitation remained very low (as confirmed by TEM observation of specimens after creep). In such conditions, tertiary creep was not reached and the cavitation term can be neglected in the above equation.

Therefore, as illustrated by Fig. 14, the total strain can be considered to result from:

- a recoverable viscoelastic contribution modeled by two K–V elements in series with a

spring which represents SiC pinning the grain boundaries and counteracting sliding;
- a permanent contribution that can be schematically drawn by a dashpot in parallel with a slider.

The dashpot represents the plastic deformation of grains through a lattice mechanism based on dislocation motion whereas the slider corresponds to the threshold stress value above which dislocation motion is activated.

However, the difference between the viscoelastic curves during loading and unloading observed for the 1st and the 2nd cycles cannot be explained by only considering these two creep contributions and an additional non-linear transient phenomenon must be added.

Taking into account the hardening phenomenon highlighted by the elastic strain decrease with increasing number of cycles, it is proposed to relate this transient phenomenon to the presence of badly aligned grains, of grains pinned by SiC particles or even by grain boundaries progressively depleted in residual glassy phase (depending on grain boundary orientation, glassy phase can be squeezed out when deformation proceeds). All those microstructural features inhibit creep by progressively impeding grain sliding and rearrangement and give rise to the formation of a stiff network. Once this process is completed, the discrepancy between viscoelastic creep during loading and recovery disappears as illustrated by Fig. 7. At this stage, as shown by TEM micrograph (Fig. 13), grain boundary sliding can only continue under the condition that stresses associated with sliding are relaxed by plastic deformation of the grains.

If such a deformation mechanism is adopted, addition of nano-sized SiC particles is no longer a necessary condition in order to obtain a significant improvement of the creep behaviour compared with monolithic alumina. Indeed, high creep resistance

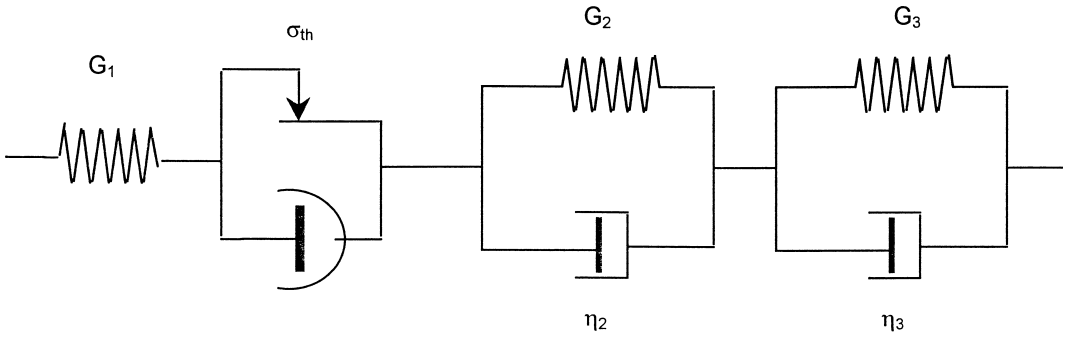

Fig. 14. Diagram of the model adopted to explain nanocomposite creep behaviour.

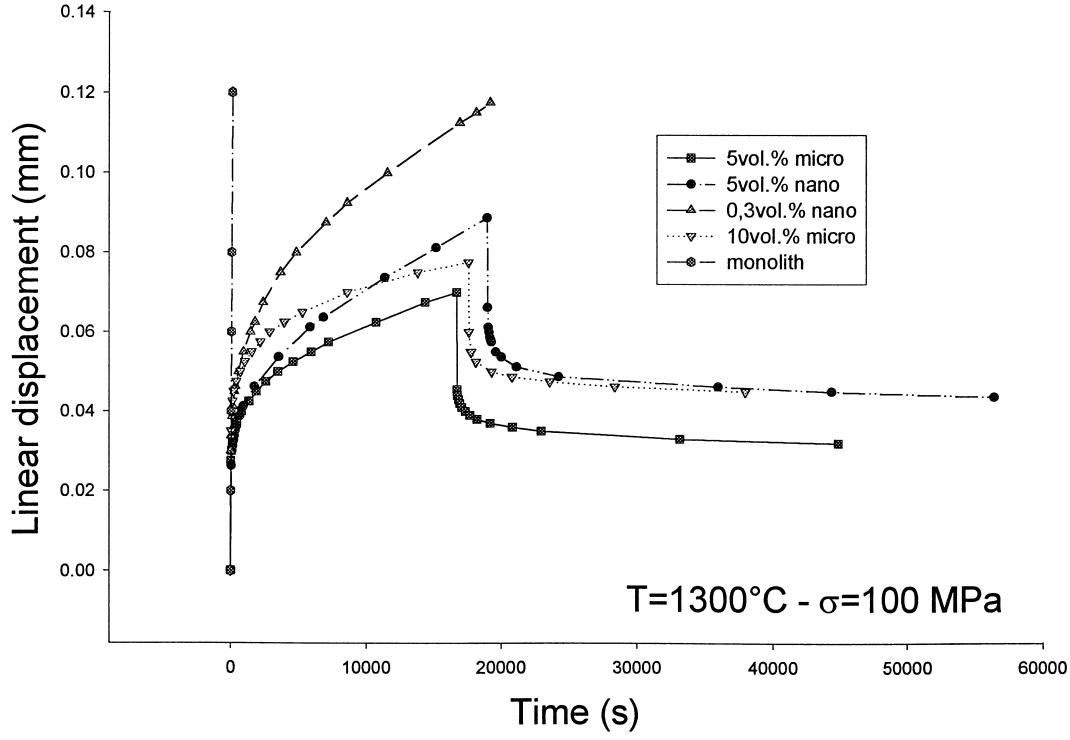

Fig. 15. Flexural creep curves relative to monolithic alumina as well as nano- and microcomposites: (1300°C, $\sigma = 100$ MPa).

could also be expected when adding micron-sized particles provided that the matrix grains were coarse enough to ensure grain boundary bridging by a large number of SiC grains. On that basis, Al_2O_3 composites containing various contents either of nanometer or micron (0·98 μm UF10-HC Starck) sized SiC have been fabricated by the processing route described in Section 2.1, in order to assess their creep behaviour.

The composite composition as well as some of their microstructural characteristics such as grain size (measured both by an intercept method and by image analysis) and the number of bridging particle per grain are included in Table 1.

Curves relative to each composite (tested in the following conditions: $T = 1300°C$, $\sigma = 100$ MPa) are presented in the same curve for ease of comparison (Fig. 15).

Examination of these curves, clearly shows:

- That incorporation of a very low amount of SiC nano particles (0·3 vol%) is apparently sufficient to markedly lower the creep strain compared with the monolithic material. This observation is not surprising if it is considered that this composite, as well as all those included in Table 1, displayed transgranular fracture at room temperature compared with intergranular fracture in monolithic alumina.
- That the 10 vol% SiC microcomposite, which contained the largest number of SiC particles pinning grain boundaries had the highest creep resistance in spite of its relatively small grain size.
- That, by comparison of 5 vol% nano and microcomposites, the creep resistance is governed by two counteracting effects: a large number of bridging SiC particles induces the formation of stiff clusters therefore increasing the 'apparent' grain size (favourable for creep resistance) but, in turn, SiC particles tend to inhibit grain growth which facilitates deformation.

All these observations confirm that addition of particles of nanometer size is not a necessary condition to obtain high creep resistant materials, and that by carefully tailoring the microcomposite microstructure (to promote location of SiC at grain boundaries), it is possible to obtain similar or even lower strain levels.

Table 1. Grain size and number of bridging particles per grain of alumina-based composites reinforced with various amounts of either nano- or micro particles

	Matrix grain size (μm)		
Material	*Intercept method*	*Image analysis*	*Number of particles bridging the GB*[a]
5 vol% nano	0·5	0·5	1·5
5 vol% micro	3·5	3·8	0·9
0·3 vol% nano	4·1	4·4	0·2
10 vol% micro	1·5	1·7	2·0

[a]In the plane of the TEM micrographs.

4 Conclusions

A deformation mechanism is proposed for Al_2O_3–SiC nanocomposite.

The main factor controlling strain appears to be SiC nanoparticles pinning the grain boundaries with, as a consequence:

- a decrease in grain boundary sliding
- a viscoelastic contribution to creep
- an enhancement of the grain boundary strength allowing plastic deformation of grains through dislocations motion.

In addition, due to the presence of non-bridged grain boundaries, the applied stress causes initial deformation by grain sliding and rearrangement of the microstructure. Such rearrangement can proceed until badly aligned grains or grain boundaries either pinned by SiC particles or depleted in glassy phase are encountered. When this occurs rearrangement is stopped and only lattice mechanisms based on dislocation motion, and to a lesser extent, a viscoelastic mechanism still contribute to the creep process.

The sliding rearrangement phenomenon is transient in nature and in addition to the viscoelastic behaviour explains therefore why under a given temperature the steady state stage is delayed for nanocomposite materials. The proposed deformation mechanism which is mainly based on increased bonding between grains, is also in agreement with the room temperature mechanical properties as well as with the wear and the machining behaviours. Indeed, such a mechanism necessarily promotes strengthening at the expense of toughening mechanisms, such as crack deflection or microcracking, both involving propagation of the main crack along the grain boundaries. As a consequence, an especially large increase of the modulus of rupture and a change in the fracture mode which becomes transgranular are observed.

In the same way, grain pull out during machining or during erosive wear is considerably reduced and the wear rate is no longer grain-size dependent.

Finally, it is pointed out that the suggested deformation process predicts that incorporation of micron-sized SiC particles in place of nano-sized SiC should also result in an increase in creep resistance of the same order of magnitude, which has been confirmed experimentally. The lower cost of micron-sized particles and their easier dispersion

would suggest that such materials would be more suitable as creep resistant materials.

Acknowledgements

Financial support of the project under Brite-Euram contract BRE CT 92 0358 (Benacomp) by European Commission is gratefully acknowledged.

References

1. Niihara, K. and Nakahira, A., Particulate strengthened oxide nanocomposites. In *Advanced Structural Inorganic Composites, Elsevier Science*, ed. P. Vincenzini. Elsevier Science, Trieste, Italy, 1990, pp. 637–664.
2. Niihara, K., New design concept of structural ceramics–ceramic nanocomposites. *J. Ceram. Soc. Jpn*, 1991, **99**(10), 974–982.
3. Deng, Z. Y., Shi, J. L., Zhang, Y. F., Jiang, D. Y. and Guo, J. K., Pinning effect of sic particle on mechanical properties of Al_2O_3–SiC ceramic matrix composites. *J. Eur. Ceram. Soc.*, 1998, **18**, 501–508.
4. Ohji, T., Nakahira, A., Hirano, T. and Niihara, K., Tensile creep behavior of alumina/silicon carbide nanocomposites. *J. Am. Ceram. Soc.*, 1994, **77**(12), 3259–3262.
5. Davidge, R. W., Brook, R. J., Cambier, F., Poorteman, M., Leriche, A., O'Sullivan, D., Hampshire, S. and Kennedy, T., Fabrication, properties and modelling of engineering ceramics reinforced with nanoparticles of silicon carbide. *British Ceram. Trans.*, 1997, **96**(3), 121–127.
6. Ohji, T., Jeong, Y. K., Choa, Y. H. and Niihara, K., Strengthening and toughening mechanisms of ceramic nanocomposites. *J. Am. Ceram. Soc.*, 1988, **81**(6), 1453–1460.
7. Levin, I., Kaplan, D. and Brandon, D. G., Effect of submicrometer particle size and content on fracture toughness of alumina–SiC "nanocomposites". *J. Am. Ceram. Soc.*, 1995, **78**(1), 254–256.
8. Sternitzke, M., Review: structural ceramic nanocomposites. *J. Eur. Ceram. Soc.*, 1997, **17**, 1061–1082.
9. Ohji, T., Hirano, T., Nakahira, A. and Niihara, K., Particle/matrix interface and its role in creep inhibition in alumina/silicon carbide nanocomposite. *J. Am. Ceram. Soc.*, 1997, **79**(1), 33–45.
10. Zhao, J., Stearns, L. C., Harmer, M. P., Chan, H. M., Miller, G. A. and Cook, R. F., Mechanical behavior of Al_2O_3–SiC "nanocomposites". *J. Am. Ceram. Soc*, 1993, **76**(2), 503–510.
11. Davidge, R. W., Twigg, P. C. and Riley, F. L., Effects of silicon carbide nano-phase on the wet erosive wear of polycrystalline alumina. *J. Eur. Ceram. Soc.*, 1996, **16**, 799–802.
12. Hollenberg, G. W., Terwillger, G. R. and Gordon, R. S., Calculation of stresses and strains in four-point bending creep tests. *J. Am. Ceram. Soc.*, 1971, **54**(4), 196–199.
13. Hvizdos, P., Dusza, J. and Rudnoyova, E. Deformation in Si_3N_4–Si_3N_4 whisker and Al_2O_3–SiC whisker composite ceramics. In *Fourth Eur Ceramics*—Vol. 3, ed. S. Meriani and V. Sergo. Pub. Gruppo Editoriale Faenza Editrice S.p.A., Faenza, Italy, 1995, pp. 205–210.
14. Gu, W., Porter, J. R. and Langdon, T. G., Evidence for anelastic creep recovery in silicon carbide-whisker-reinforced alumina. *J. Am. Ceram. Soc.*, 1994, **77**(6), 1679–1681.
15. Pierard, J. M., Modéles et fonctions visco-elastiques linéaires. In *La Rhéologie*, ed. B. Persoz. Mason et Cie, Paris, 1969, pp. 19–44.
16. Morrell, R. and Ashbee, K. H. G., High temperature creep of lithium zinc silicate glass-ceramic—part 2: compression creep and recovery. *J. Mater. Sci.*, 1974, **8**, 1271–1277.
17. Arons, R. M. and Tien, J. K., Creep and strain recovery in hot-pressed silicon nitride. *J. Mater. Sci.*, 1980, **15**, 2046–2138.
18. Couarraze, G. and Grossiord, J. H., *Initiation à la Rhéologie*, Pub. Technique et documentation. Lavoisier, Paris, France, 1983, p. 48.
19. Canon, R. M., Rhodes, W. H. and Heuer, A. H., Plastic deformation of fine-grained alumina (Al_2O_3): I, interface-controlled diffusional creep. *J. Am. Ceram. Soc.*, 1980, **63**(1-2), 46–52.
20. Chokshi, A. H. and Porter, J. R., High temperature mechanical properties of single phase alumina. *J. Mater. Sci.*, 1986, **21**, 705–710.
21. Minden, C. V. and Hübner, H., Creep of platelet-reinforced ceramics. In *Third Euro Ceramics* Vol.3, ed. P. Durran and J. F. Fernandez. Faenza Editrice Iberica, Castellion, Spain, 1993, pp. 671–676.
22. Lin, H.-T. and Becher, P. F., Creep behaviour of a SiC-whisker reinforced alumina. *J. Am. Ceram. Soc.*, 1990, **73**, 1378–1381.
23. Chokshi, A. H. and Porter, J. R., Creep deformation of an alumina matrix composite reinforced with silicon carbide whiskers. *J. Am. Ceram. Soc.*, 1985, **68**, C144–145.
24. Jiao, S., Jenkins, M. L. and Davidge, R. W., Interfacial fracture energy-mechanical behaviour relationship in Al_2O_3–SiC and Al_2O_3–TiN nanocomposites. *Acta Mater.*, 1997, **45**, 149–156.
25. Cannon, W. R. and Langdon, T. G., Review creep of ceramics—Part 1: mechanical characteristics. *J. Mater. Sci.*, 1983, **18**, 1–50.
26. Cannon, W. R. and Langdon, T. G., Review creep of ceramics. Part 2–an examination of flow mechanisms. *J. Mater. Sci.*, 1988, **23**, 1–20.
27. Lange, F. F., Davis, B. I. and Clarcke, D. R., Compressive creep of Si_3N_4/MgO alloys—Part 2: source of viscoelastic effect. *J. Mater. Sci.*, 1980, **23**, 611–615.